Taylor & Francis
Taylor & Francis Group

AVIATION
ISSN 1648-7788 / eISSN 1822-4180
2014 Volume 18(3): 109–119
doi:10.3846/16487788.2014.969885

NUMERICAL ANALYSIS OF FLIGHT CONDITIONS AT THE ALTA AIRPORT, NORWAY

Adil RASHEED, Asif MUSHTAQ

Applied Mathematics, SINTEF ICT, Strindaveien 4, Trondheim, Norway
E-mail: adil.rasheed@sintef.no (corresponding author)

Received 11 April 2013; accepted 20 August 2014

Adil RASHEED, *PhD*
Research Scientist– applied mathematics, SINTEF ICT, Norway since 2009.
PhD – LESO-PB, EPFL, Switzerland 2005–2009.
MSc – Mechanical Engineering, IIT Bombay, India 2000 to 2005.
Research interests: aviation safety, wind energy, turbulence modeling, CFD.

Asif MUSHTAQ, *PhD*
Research Scientist– applied mathematics, SINTEF ICT, Norway; Research Scientist – Department of Mathematical Sciences, NTNU, Trondheim Norway. PhD – Norwegian University of Science and Technology (NTNU), Trondheim Norway (2010–2014). M.Phil (applied mathematics), Govt. College University (GCU) Lahore, Pakistan (2006–2009). MSc (computational mathematics), University of the Punjab, Lahore Pakistan (1998–2000). Research interests: differential equations and numerical analysis, higher order symplectic integrators, hamiltonian systems, CFD, wind energy forecasting, data analysis.

Abstract. In this paper, the results from a numerical study of the atmospheric flow characteristics at the Alta airport, Norway are presented. Experiences of the pilots operating in the region have been used to validate the findings. Further analysis has resulted in the identification of dangerous zones for aviation activities for a particular wind direction. Towards the end an effort has been made to relate the experience of the pilots with the mountain waves generated due to the presence of a small hill close to the airport.

Keywords: aviation safety, terrain-induced turbulence, atmospheric flow.

1. Introduction

Flow in a hilly region is characterized by a high level of turbulence and wind shears, resulting from rotor formations and flow separations. In particular during takeoff and landing aircrafts operating in hilly regions are subjected to atmospheric disturbances. The disturbances have a great influence on the characteristics, comfort and safety of the flight. Every year a number of incidents and accidents linked to turbulence and wind shear are reported (Plane Crashinfo 2013). In order to prevent such incidents, a numerical code based on the governing equations of mass, momentum and energy conservation have been developed. In the present paper we apply the numerical code to simulate flow close to Alta airport in the northern part of Norway. Since it is rarely possible to obtain reliable data to carry out a quantitative validation, we have restricted ourselves to reproducing the experiences of the pilots operating in the region. A more quantitative study applying the same numerical tool for wind engineering applications has been reported in (Eidsvik 2005). However, the authors expect that the tool can be effective for the analysis of turbulence related risk in aviation activities, as well as for forecasting turbulence to create an alert.

2. Theory

2.1. Model description

The code used for the present simulation is called SIMRA and is based upon the Reynolds-averaged equations with standard $(k-\varepsilon)$ turbulence closure. It has the capability of predicting flows with separation, attachment, hydraulic transition, internal wave breaking and mountain waves. It has the ability to dynamically estimate the turbulent kinetic energy and dissipation. The square root of turbulent kinetic energy has the dimension of velocity and is a good representation of turbulence. The governing equations of mass, momentum, energy, turbulent kinetic energy and dissipation are solved using the finite element method. More details, description and validation results can be found in (Utnes 2007a, 2007b; 2008).

2.2. Governing equations

The equation of motion for incompressible flow may be generalized to atmospheric flows by the use of the anelastic approximation. This formulation is often applied in meteorological models, and may be written in the following conservative form (Bannon 1995) and (Durran 1998).

$$\nabla(\rho_S u)=0\,; \tag{1}$$

$$\frac{Du}{Dt}=-\nabla\left(\frac{p_d}{\rho_S}\right)+g\left(\frac{\theta_d}{\theta_S}\right)+\frac{1}{\rho_S}\nabla(\tau)+f\,; \tag{2}$$

$$\frac{D\theta}{Dt}=\nabla(\gamma\nabla\theta)+q\ . \tag{3}$$

Here (u,p,θ,ρ) represent velocity, pressure, potential temperature and density, respectively. Furthermore, τ is the stress tensor, f is a source term that may include rotational effects, g is the gravitational acceleration, γ is the thermal diffusivity, and q is the energy source term. Subscript s indicates hydrostatic values and subscript d – the deviation between the actual value and its hydrostatic part, i.e. $p=p_S+p_d, \theta=\theta_S+\theta_d, \rho=\rho_S+\rho_d$, where the hydrostatic part is given by $\partial p_S/\partial z=g\rho_S$. Additionally, the following expression for hydrostatic density may be derived from the state equation and the definition of potential temperature:

$$\rho_S=\frac{p_S}{R\theta_S}\left(\frac{p_0}{p_S}\right)^{R/C_p}\ , \tag{4}$$

where R is the gas constant and C_p is the specific heat at constant pressure. Hence, once the hydrostatic (potential) temperature profile is given, the hydrostatic pressure and density may be calculated, and then substituted into Equations (1) and (2).

It must be noted that the Boussinesq approximation is obtained from the system of Equations (1) and (2) by assuming constant values (ρ_0,θ_0) instead of the hydrostatic values, and this formulation may well be used for incompressible flow and ordinary temperature.

The aim of the present study is to solve these equations for high-Reynolds number flows. For this purpose unsteady Reynolds-averaged modeling of the equation system, together with a turbulence model is applied. Presently a standard high-Reynolds $(k-\varepsilon)$ turbulence model is used for this purpose. With these assumptions the model equations take the following form:

$$\nabla(\rho_S u)=0\ ; \tag{5}$$

$$\frac{Du}{Dt}=-\nabla\left(\frac{p_d}{\rho_S}\right)+g\left(\frac{\theta_d}{\theta_S}\right)+\frac{1}{\rho_S}\nabla(\tau)+f\ ; \tag{6}$$

$$\frac{D\theta}{Dt}=\nabla(\gamma\nabla\theta)+q\,; \tag{7}$$

$$\frac{DK}{Dt}=\nabla(\nu_T\nabla K)+P_k+G_\theta-\varepsilon\,; \tag{8}$$

$$\frac{D\varepsilon}{Dt}=\nabla\left(\frac{\nu_T}{\sigma_e}\nabla\varepsilon\right)+(C_1P_k+C_3G_\theta)\frac{\varepsilon}{k}-C_2\frac{\varepsilon^2}{k}\,, \tag{9}$$

where turbulent viscosity is given by $\nu_T=C_\nu\frac{k^2}{\varepsilon}$. The Reynolds stress tensor is given by

$$R_{ij}=\nu_T\left(\frac{\partial u_i}{\partial x_j}+\frac{\partial u_j}{\partial x_i}\right)-\frac{2}{3}k\delta_{ij}\,, \tag{10}$$

while the eddy diffusivity appearing in the energy equation is $\gamma_T=\nu_T/\sigma_T, \sigma_T$ being the turbulent Prandtl number. The production and stratification terms in the turbulence model are given by

$$P_k=\nu_T\left(\frac{\partial u_i}{\partial x_j}+\frac{\partial u_j}{\partial x_i}\right)\frac{\partial u_i}{\partial x_j}, G_\theta=-\frac{g}{\theta}\frac{\nu_T}{\sigma_T}\frac{\partial\theta}{\partial z}\,. \tag{11}$$

Conventional constants for the high-Reynolds $(k-\varepsilon)$ model are given by

$$(C_\nu,C_1,C_2+\sigma_\theta)=(0.09,1.44,1.92,1.3)\,. \tag{12}$$

The value for C_3 is more uncertain. In the present study we assume that $C_3G_\theta=\max(G_\theta,0)C3G\theta$, i.e. $C_3=0$ in stably stratified flows, elsewhere $C_3=1$. (Rodi 1987).

2.3. Safety analysis

The simplest meteorological variable considered to be most important for aviation safety is called the F-factor or wind shear and what is called turbulence, represented by $\varepsilon^{1/3}$. These quantities are given by Equations (13) and (14)

$$F=-\overline{\frac{c}{g}\frac{\partial u}{\partial x}\frac{w^{l_f}}{c}}\,;$$

$$F=-\frac{c}{g}[u(x+l_f/2-u(x-l_f/2)+\frac{w^{-l_f}}{c}]\,; \tag{13}$$

$$\varepsilon^{1/3}\approx\left(\frac{C_\mu^{1/2}K}{l_t}\right)\approx 0.67K^{1/2}l_t^{1/3}\ . \tag{14}$$

Here c is the fly path, g – the acceleration due to gravity, u – the wind component along the fly path, w – the

vertical wind component, ε – the turbulent dissipation, K – turbulent kinetic energy, l_t – turbulent length scale and l_f – the minimum response distance for landing configuration and is of the order of $\sim 500\,\mathrm{m}$, which corresponds to a time interval of about $t = O(7s)$. Averaging over this distance is indicated by an overline. Coefficient C_μ is taken as $C_\mu = 0.09$. A good review of this theory can be found in the paper by K. Eidsvik *et al.* (2004).

Prevalence of the two conditions $F < -0.1$ and $\varepsilon^{1/3} > 0.5\,\mathrm{m}^{2/3}\mathrm{S}^{-1}$ corresponds to severe turbulence for commercial aircraft and represents potential danger (Clark *et al.* 1997). These conditions are easily met when $\sqrt{K} > 3\,\mathrm{ms}^{-1}$.

2.4. Mountain waves

Buoyancy perturbations develop when stably stratified air ($d\theta/dz > 0, \theta$ being the potential temperature) ascends a steep mountain barrier. These perturbations often trigger disturbances that propagate away from the mountain as gravity (or buoyancy) waves. These waves triggered by the flow over a mountain are referred to as mountain waves. Large-amplitude mountain waves can generate regions of clear-air-turbulence that pose a hazard to aviation. A relevant non-dimensional number to characterize mountain waves is the Froude number, which is defined as

$$Fr = \frac{U}{NL}, \tag{15}$$

where U is reference velocity and L – reference length. N is the buoyancy frequency given by

$$N^2 = \frac{g}{\theta}\frac{d\theta}{dz}. \tag{16}$$

The relevant quantities of mountain waves are the free stream wind velocity, vertical potential temperature profile, and mountain width or height distributing the flow, or, actually, the natural length of the mountain(s) that can create an internal wave of a $2L$ wavelength. Mountain waves may occur if the actual Froude number is of the order of one: $Fr = O(1)$. A detailed behavior of these waves can be found in J. Doyle and D. Durran (2001). In the case of Alta, the terrain is highly uneven and propagation of these waves could not be ignored without an investigation. Therefore, their nature was also analyzed.

3. Location, terrain and observed wind condition at the site

Alta Airport is the airport of Alta, Norway. It is located about 4 km northeast of the town center of Alta, near the community Elvebakken on the southern shore of the Altafjord (Fig. 1). The airport has a single paved 2,088 m runway. With 334,132 passengers served in 2009, it is the busiest airport in Finnmark according to passenger traffic. The airport works as a semi-hub for operations in the SAS Group with many connections to regional airports in Finnmark. It is served with Boeing 737 aircraft to Oslo by Norwegian Air Shuttle and Scandinavian Airlines, and by the latter to Tromsø. Widerøe operates many of its regional services through Alta. The airport can handle non-Schengen flights in a designated section of the terminal building, although since March 2010 no international flights to Alta Airport are in operation. Alta is situated on a plain where the Alta River flows into the fjord. In a somewhat greater distance, especially in the north-west, west and south-west there are mountains with elevations up to about 1000 m.

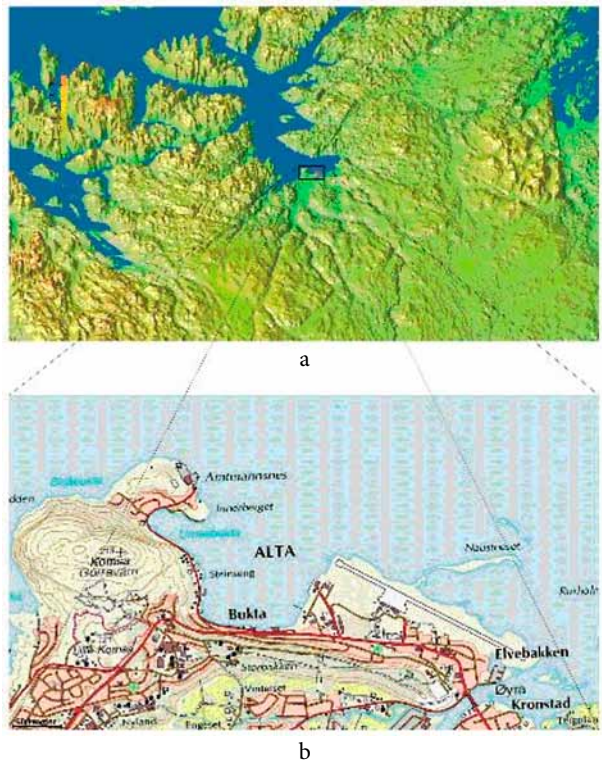

a

b

Fig. 1. (a) Terrain in the vicinity of the airport. The runway is marked by a red strip in the middle of the figure. (b) A close-up of the Alta airport with the Komsa hill

To the south-east of the airport the terrain is relatively flat and the presence of the Alta fjord on the north-west side makes this direction an ideal one for takeoff or landing. It is not surprising that the runway is aligned in this direction.

Reports by pilots flying to and from Alta airport tell that strong turbulence occasionally occurs with south-westerly (SW) wind at 20 to 25 m/s, in particular between 600 and 3000 m above sea level. Also, pilots report that dissimilar wind conditions on the runway can sometimes cause landing problems, in particular, with wind from between SSW and NW at strength of 20 m/s or more. A corresponding flight path plotted using the flight data is presented in figure 2.

To study the details of the structure of local airflow and turbulence in the region near Alta airport, a set of different wind effects are simulated and analyzed. The study concentrates on the above mentioned wind directions.

The wind rose diagram in figure 3 shows the seasonal variation of wind strength and direction. It is clear from the figure that during spring, autumn and winter wind from the south-east direction is the most dominant.

Fig. 2. Flight path from the pilots' report

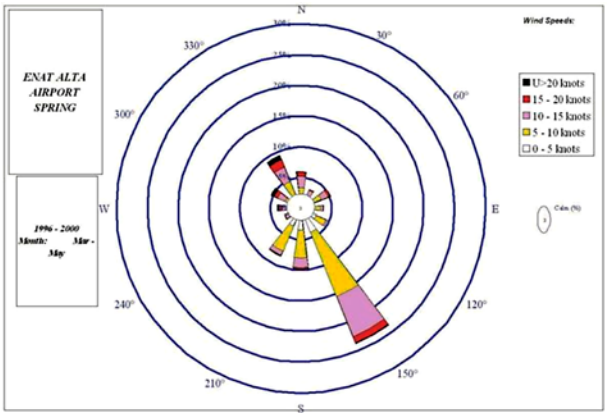

(a) Spring

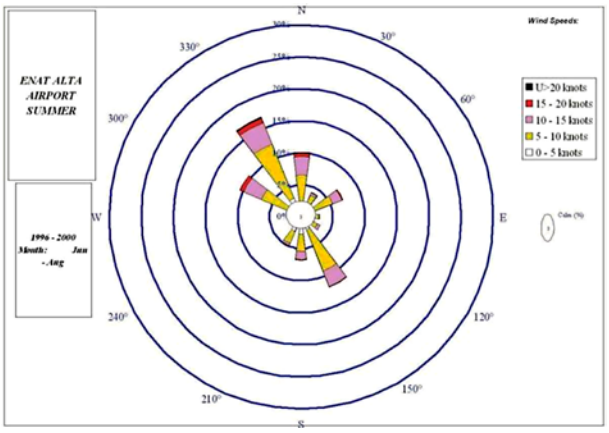

(b) Summer

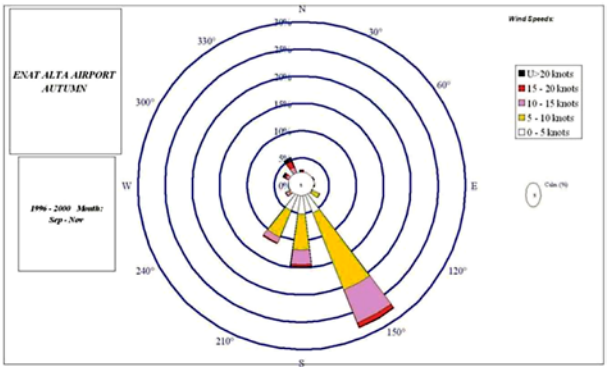

(c) Autumn

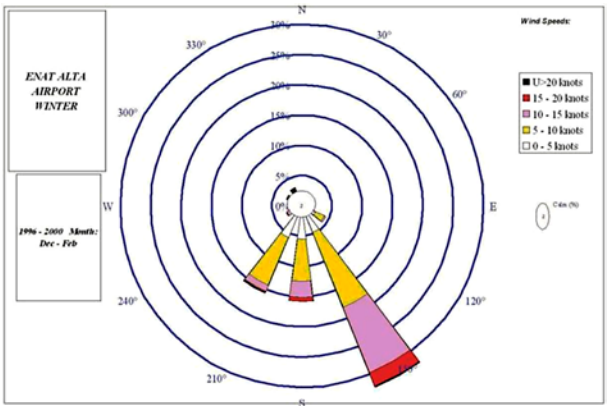

(d) Winter

Fig. 3. Seasonal wind rose diagrams for Alta airport

However, during summer, there is a complete reversal of the wind direction due to the suction effect created by warmer inland surfaces. The magnitude of these winds varies between 2.5 m/s and 10 m/s. However, according to the pilot reports the magnitude can very easily reach 25 m/s (free stream wind speed) or more, occasionally, in which case strong turbulence is experienced at the altitude between 600 and 3000 m. The wind rose diagram in figure 4 shows the annual variation of wind strength and direction.

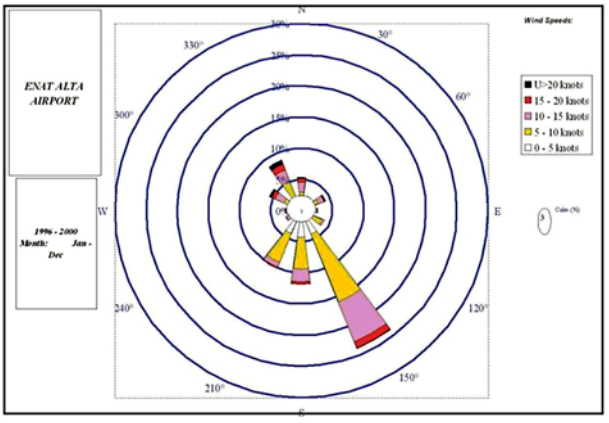

Fig. 4. Annual wind rose diagram for Alta airport

4. Simulation setup

As was already discussed, terrain induced turbulence is known to be problematic near the airport, especially if there is a southeasterly wind. To simulate these effects we use the terrain data of the area of interest and generate an unstructured hexahedral mesh for it in such a way that the vertical mesh lines are normal to the ground surface. More details regarding the domain size, terrain, mesh, boundary conditions and simulations are provided in the following sub-sections.

4.1. Safety analysis

Terrain data (Fig. 1) for the area in the vicinity of the airport is available at a resolution of 100 m. This puts a constraint on the finest resolution that could be used for the study as any finer resolution would imply an interpolation of the terrain data. The horizontal expanse of the domain was $30\,\text{km} \times 30\,\text{km}$ with the airport occupying almost the central position as shown in figure 5(a). The mesh was intentionally refined in the vicinity of the airport (giving a resolution of about 50 km for a 300×300 mesh in horizontal directions (Fig. 5(b)). Since terrain data is not available at this resolution, interpolation was unavoidable.

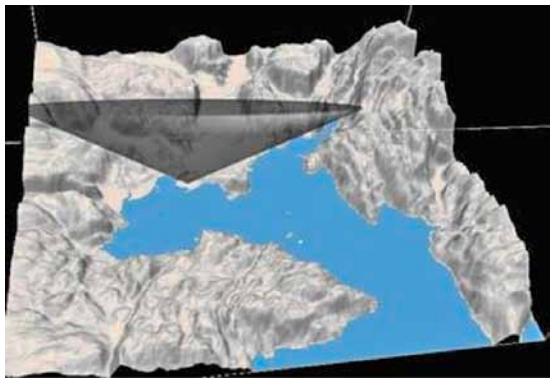

(a) Terrain and the cone containing the gliding path

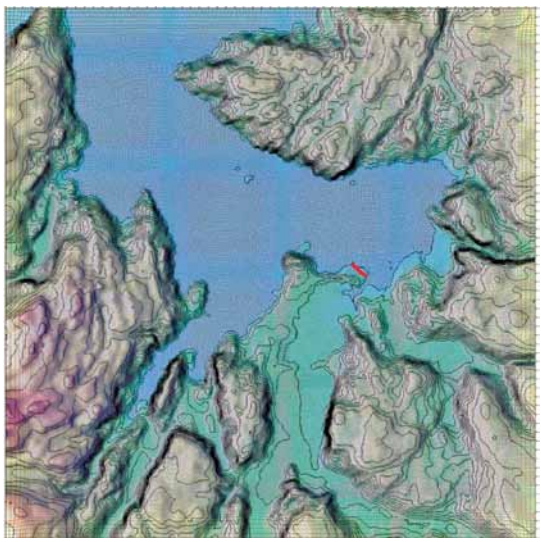

(b) Mesh: 300×300

Fig. 5. Alta: domain size is 30 km×30 km and horizontal resolution ranges from 50 m near the airport to 150 m near the boundary of the domain. The runway is marked by a red strip

However, with the terrain close to the airport being relatively flat (except for the Komsa hill area) the error induced due to such an interpolation is expected to be insignificant. In the vertical direction 41 levels with a stretching factor of 1.1 were used to discretize a vertical expanse of 3000 m. This resulted in a vertical resolution of 3 m near the ground and 3000 m near the top of the domain.

4.2. Boundary conditions

In complicated mountainous terrain it is generally difficult to specify a realistic inlet profile. Therefore, a standard profile for wind speed and turbulent kinetic energy was used to specify the boundary conditions and initialize the domain.

The profiles for the wind speed $u_0(z)$ and the turbulent kinetic energy $K_0(z)$ are obtained by

$$u_0(z) = \frac{u_*}{\kappa}\left(\ln\frac{z}{z_0} + W\left(\frac{z}{D}\right)\right); \tag{17}$$

$$K(z) = C_\mu^{1/2} u_* \left(1 - \frac{z}{D}\right), \tag{18}$$

where u_*, z_0, z and D represent friction velocity, surface roughness, height above the ground surface and boundary layer thickness, respectively. The so-called wake function W is defined by the formula:

$$W\left(\frac{z}{D}\right) = (A-1)\left(\frac{z}{D}\right) - \frac{A}{2}\left(\frac{z}{D}\right)^2, \text{ therefore } W(1) = 1.$$

The coefficients are $\kappa = 0.42$ and $A = 4.0$. Synoptic wind (mesoscale) U is given by $U = u_0(D)$. In the present simulations we have used $(z_0, D, U) = (0.3\,\text{m}, 1500\,\text{m}, 20\,\text{m/s})$ so that the friction velocity $u_* \approx 0.9\,\text{m/s}$ and wind speed 10 m above the ground is $u_0 \approx 7.5\,\text{m/s}$. A surface roughness value of 0.001 has been used for the sea surface. Along with the magnitude, the direction of the synoptic wind is also specified. Several simulations were conducted for different wind directions. The convention used to specify wind direction α in this report is demonstrated in figure 6(a). It should be noted that meteorology and aviation communities use a slightly different convention as shown in figure 6(b). All the simulations conducted and presented in this report are for neutral stratification (unless stated explicitly otherwise); hence, the results are scalable.

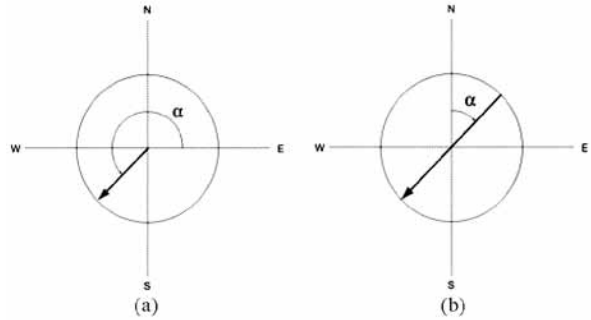

Fig. 6. Conventions for assessing wind direction. The figure shows wind from the NE. In (a) the convention we use in our simulations is shown (225°), while (b) illustrates the convention used by meteorology and aviation communities (45°)

5. Results

In this section we present the findings of the present work. Wind direction and magnitude along with the terrain are the most important factors contributing to turbulence in this region. We, therefore, categorize the findings into three subsections. First the impact of the wind direction on the turbulent intensity is presented, followed by an evaluation of the worst case scenario and finally the effects of stratification.

5.1. Effects of wind direction on the flow characteristics

Figure 7 shows turbulent velocity ($\sqrt{K}$) contours on the plane passing through the runway for four different wind directions ($\alpha = 60°, 90°, 120°, 300°$). The free stream wind speed in all four cases is 20 m/s (this should not be an issue because the results are scalable).

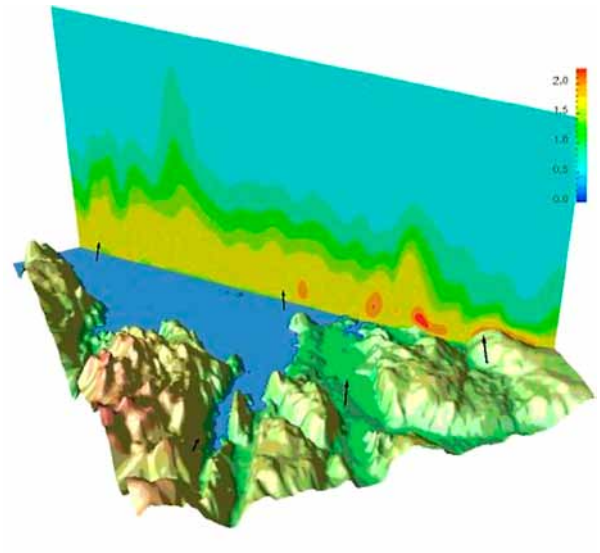

(a) 60°

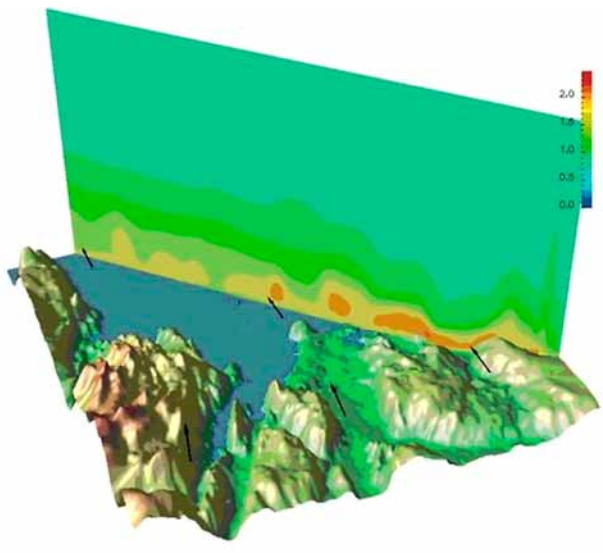

(b) 90°

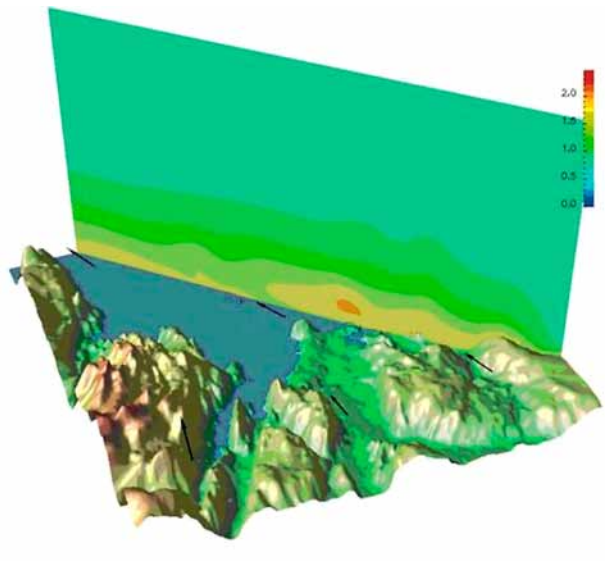

(c) 120°

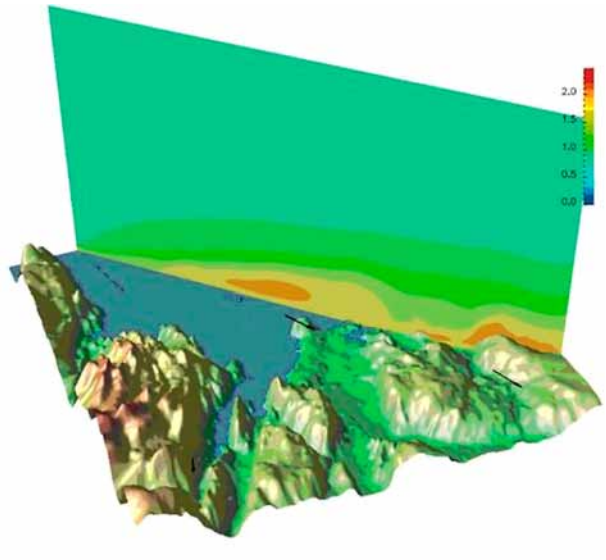

(d) 300°

Fig. 7. $\sqrt{K}$ contours on the plane passing through the runway

The worst case scenario as it appears from the simulation is when the wind blows from the SSW direction ($\alpha = 60°$). As discussed earlier, the hills to the south west of the airport extend up to a height of 1000 m. While approaching the steep hills from the south west direction the flow gains a vertical component on the windward side of the hill. Some channeling is also observed in the valleys around the hills, although the model fails to predict an expected flow separation due to low horizontal resolution. Several elongated streaks of turbulent structures, intersecting the gliding plane (Fig. 8(a)), are formed, thereby posing potential danger to flight operations. Fortunately, as observed in the wind rose diagram in figure 4, this is not the dominant wind direction and the wind speed in this direction rarely exceeds 10 m/s (corresponding to a

free stream speed of 15 m/s) obtained at the weather station located 213 m above the sea level. Although there is no serious matter of concern, a possibility of encountering an extreme condition cannot be ruled out. Also, noteworthy is the fact that significant turbulence is also predicted up to a height of 1500 m. This can probably be attributed to the more irregular terrain near the present airport under consideration.

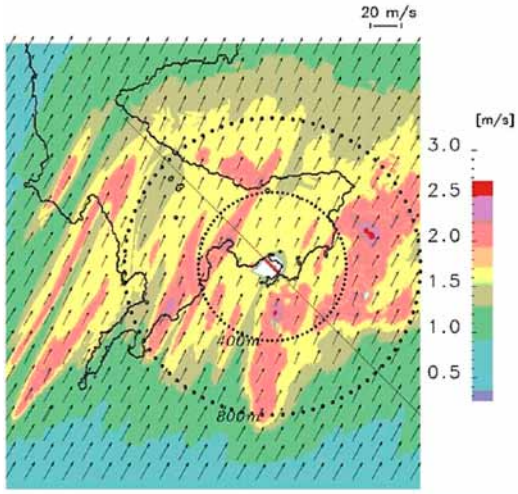

(a) $\alpha = 60°$

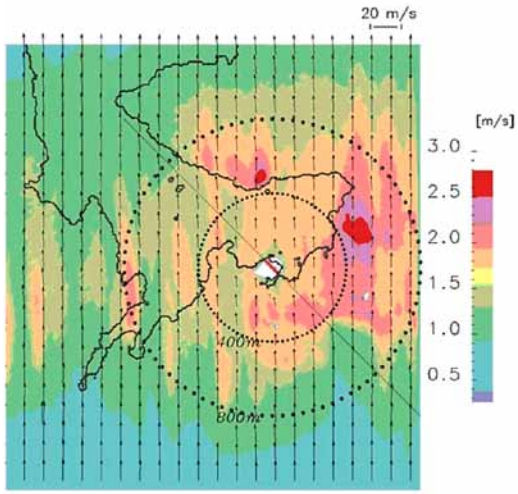

(b) $\alpha = 90°$

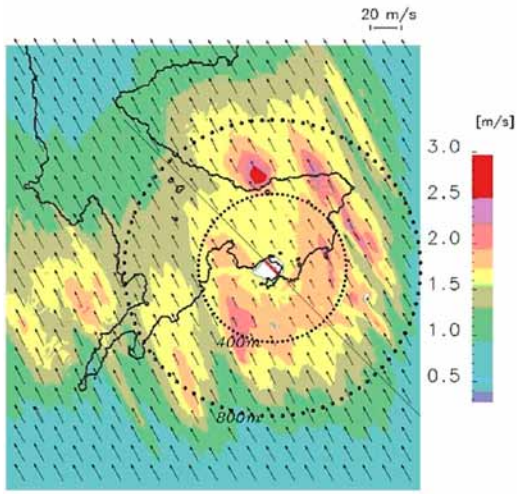

(c) $\alpha = 120°$

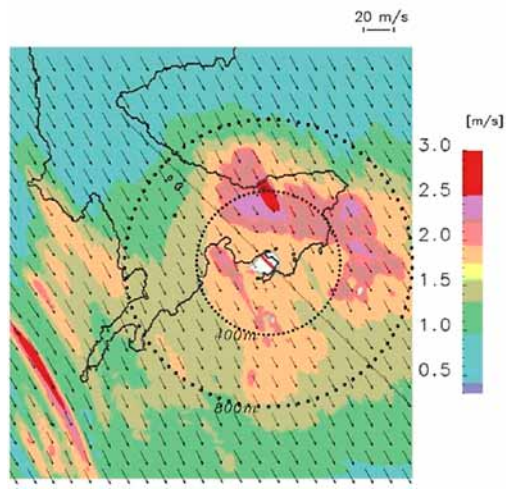

(d) $\alpha = 300°$

Fig. 8. $\sqrt{K}$ contours and the velocity field on the surface of the cone containing the gliding path (marked by a solid line)

Moreover, when the wind direction is from the SSE ($\alpha = 120°$, which is also the dominant wind direction) no high.

Topographical features are encountered by the wind before reaching the airport, this results in only a mild turbulence along the runway (Fig. 7(c)). However, a reversal of the wind direction ($\alpha = 300°$) can lead to the formation of an intense turbulent zone near the airport (Fig. 7(d)). This can be attributed to the high hills to the north of the airport. Although the frequency of occurrence of this wind direction annually is not significant, it is the dominant wind direction during summer and the free stream wind speed does reach a value of 20 m/s. Such a situation can be a matter of concern for flight operations. Wind blowing from the south leads to the formation of a highly turbulent zone on the north east side of the airport. However, flight operation can hardly be affected by these turbulent zones as they lie on the leeward side of a small hill located on the north east side of the airport.

5.2. Extreme case scenario

We define an extreme case as one in which the free stream wind speed exceeds 30 m/s. Although this situation is infrequent, it has been reported and is, therefore, considered in this report. An increase in free wind speed can lead to a significant increase in turbulence intensity. This increase can clearly be observed in figure 9. The zones which are safe at 20 m/s (located on the north of the airport) can become unsafe at higher wind speed.

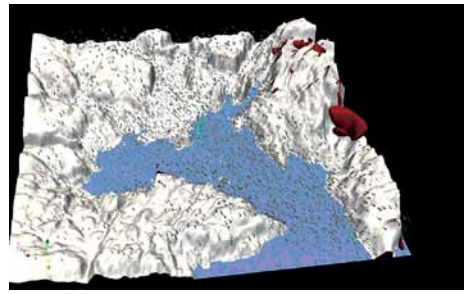

(a) $U_b = 20$ m/s

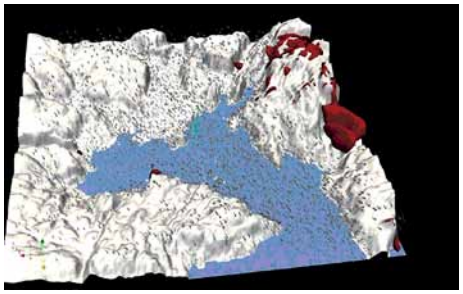

(b) U_b = 22 m/s

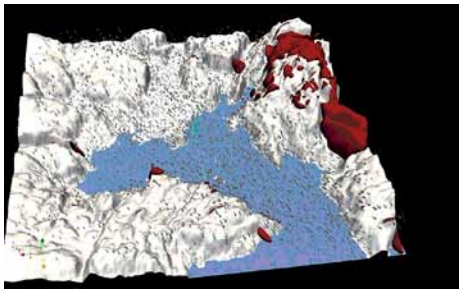

(c) U_b = 24 m/s

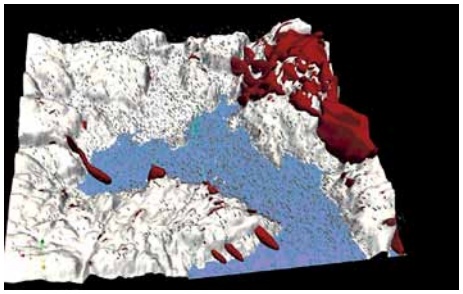

(d) U_b = 26 m/s

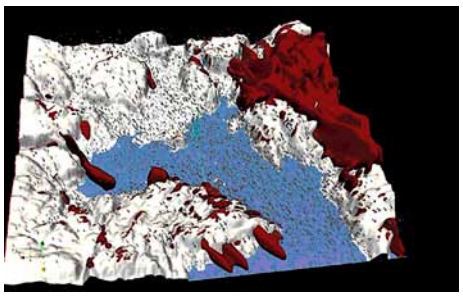

(e) U_b = 28 m/s

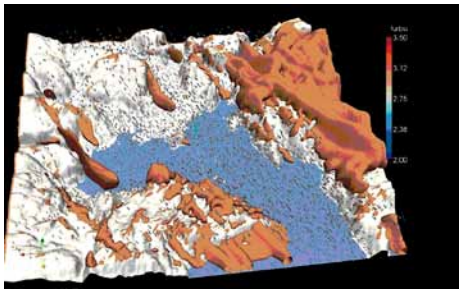

(f) U_b = 30 m/s

Fig. 9. $\sqrt{K} = 3m/s$ contour for different values of free steam wind speed

Figure 10 presents the contours of $\sqrt{K} = 3$ for the four different wind directions. From the figure it appears that the runway had been designed anticipating the turbulent zones in the vicinity. Of the four cases presented, the turbulent streaks intersect the gliding plane only for $\alpha = 60°$. In the other three cases, many more turbulent zones exist, but they are either located further away from the airport or are aligned parallel to the gliding plane. The absence of any turbulent zones above the Alta fjord facilitates the takeoff and landing along the fjord. Having said that, it should be noted that for $\alpha = 300°$ (which is the dominant wind direction during summer) highly turbulent zones are predicted very close to the gliding plane and, hence, a potential danger cannot be completely ruled out. When the wind blows from the fjord, it encounters high hills (lying to the north of the airport), which leads to the formation of zones of high turbulent kinetic energy close to the airport.

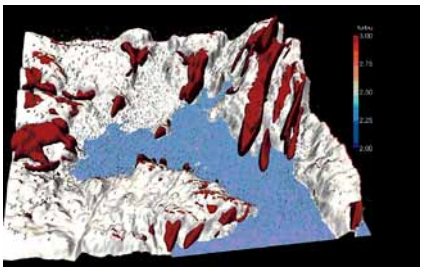

(a) α = 60°

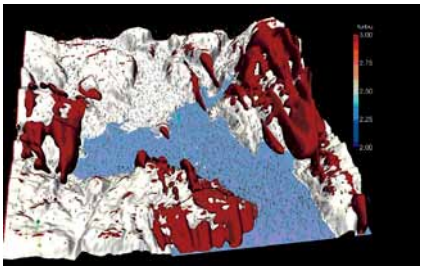

(b) α = 90°

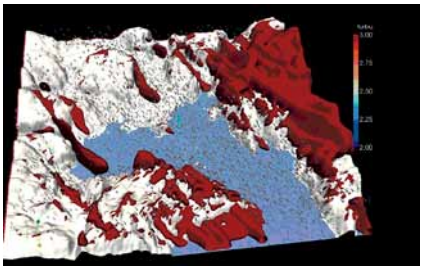

(c) α = 120°

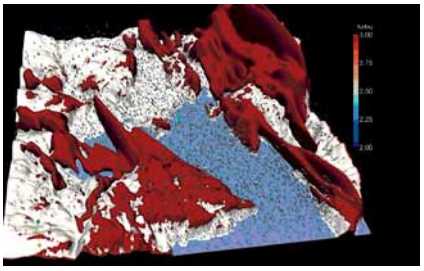

(d) α = 300°

Fig. 10. $\sqrt{K = 3m/s}$ contours for different wind directions α

5.3. Effect of stratification

For studying the mountain waves a potential temperature pro-file as shown in figure 11, which corresponds to a stable stratification, was used. This profile corresponds to $d\theta / dz = 0.009$. Wind direction $\alpha = 60°$ was chosen. This wind direction favors the formation of mountain waves. Normally, the characteristic length L in the case of an isolated hill (or mountain) is taken to be equal to the height or the horizontal width of the hill in theoretical studies.

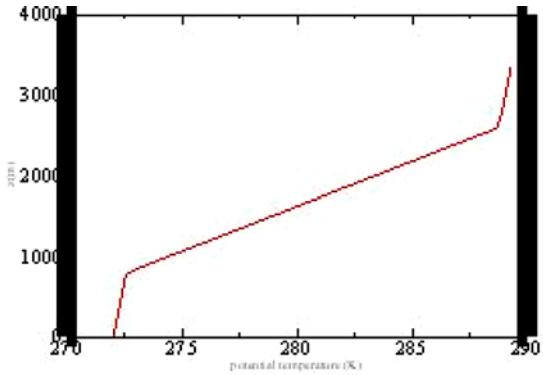

Fig. 11. Vertical potential temperature profile

In a real scenario like ours, it was difficult to decide on a proper length scale; therefore, we chose the average mountain height (O (500 m)) to define the Froud number associated with the simulation. With these two quantities fixed the Froude number could be altered by varying the free stream wind speed. With the inclusion of the effects of stratification on the momentum equation the results are no longer scalable; hence, four simulations with different free stream speeds at 10, 15, 18 and 20 m/s corresponding to the Froude number of 1.0, 1.5, 1.8, 2.0, respectively, were conducted.

A comparison of the effects of neutral and stable stratification is shown in figure 12. It appears that the stratification in this particular case dampens the turbulent kinetic energy field, especially in the upper layers, thus making conditions favorable for flight operation. Figure 13 shows the effects of Froude number variation on the turbulent kinetic energy and potential temperature profile. Mountain waves are observed for $Fr = 1.0$, but for a bigger Froude number these waves were quickly replaced by turbulent wake structures on the leeward side of the mountains. However, neither the mountain waves nor the turbulent wakes pose a real danger to aircraft as they are confined to a region far away in the valleys. In fact, we observed that at higher wind speed the stratification was actually damping the turbulence in the upper layer of the atmosphere.

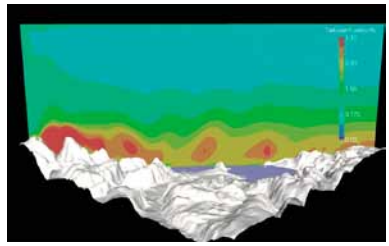

(a) Neutral Stratification

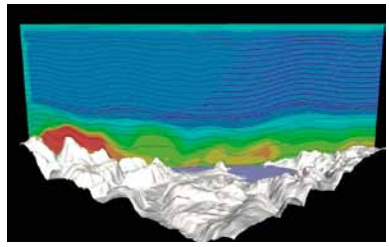

(b) Stable Stratification

Fig. 12. Effects of stratification

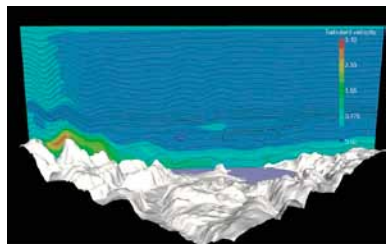

(a) $U = 10m/s, Fr \approx 1.0$

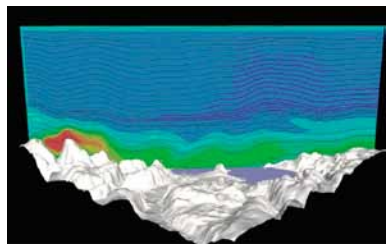

(b) $U = 15m/s, Fr \approx 1.5$

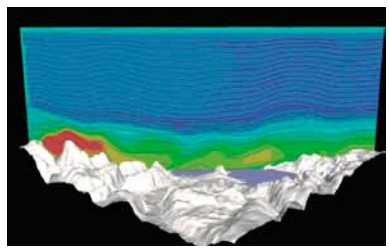

(c) $U = 18m/s, Fr \approx 1.8$

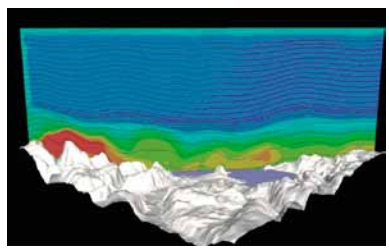

(d) $U = 20m/s, Fr \approx 2.0$

Fig. 13. Effects of stratification as a function of free stream wind speed.

6. Conclusions

In this article the findings of our study on terrain induced turbulence in and around the Alta airport have been presented. Several simulations for neutral stratification were conducted for different wind directions, and the flow characteristics were analyzed. Since the terrain and the stable stratification in the region could lead to the formation of mountain waves, their effects were also simulated for a particular wind direction of $\alpha = 60°$. Below the most important findings from the study are enumerated.

1. Confirmation of the pilots' reports. In agreement with the reports, we observed that the turbulent intensity is at a maximum for the south-westerly wind. The long streaks of high intensity turbulent kinetic energy intersect the gliding plane and can pose potential danger for aviation activities. It was also observed that, in case of a south-easterly wind, flight operations can be quite dangerous when the free wind speed reaches about 30 m/s, a value that is reached occasionally.
2. Identification of high risk zones. The study resulted in the identification of the zones where the turbulent kinetic energy can reach a maximum. It was shown that a zone that is rather quiet and safe in a calm situation (low wind speed) could turn dangerous with increasing free stream speed.
3. Evaluation of potential danger associated with mountain waves. It was found that the meteorological conditions and the topographical features (mountains) in the region facilitate the formation of mountain waves. With increasing free stream speed these mountain waves were replaced by turbulent wakes. The zones that are most affected by these phenomena were identified, and it was found that these zones were located too far from the airport to pose a real threat. In fact, it was concluded that the stratification in this region was actually damping the turbulence in the upper layers of the domain, thus facilitating flight operation.

However, there are certain issues which are worth stressing here. The first one is associated with the resolution of a small hill close to the airport. This is a situation similar to that encountered at the Tromsø airport (Utnes 2008). In Utnes study, it was observed that effects induced by a small hill were significant and very critical to the airport. In the case of Alta the situation is somewhat similar. However, owing to poor resolution of the terrain data close to the region, the effects could not be simulated. In an attempt to simulate the effects of Komsa, a small hill, on the airport in a more localized simulation using interpolated terrain data, we noticed that mountain waves generated by a combination of hill and stable stratification can, in fact, influence the airport. The vertical velocity analysis (Fig. 14) illustrates the trapped waves, producing alternating regions of subsidence and ascent well.

Considering the criticality of the issue, a more detailed and localized study with actual high resolution terrain data is required. The second point worth mentioning is the fact that the present study has concentrated on terrain-induced turbulence, which is more of a local phenomenon. A study of the effects of large-scale phenomena on the airport is beyond the capabilities of the model we used. A nested approach with different models capable of resolving different scales coupled together could be more effective for such an analysis.

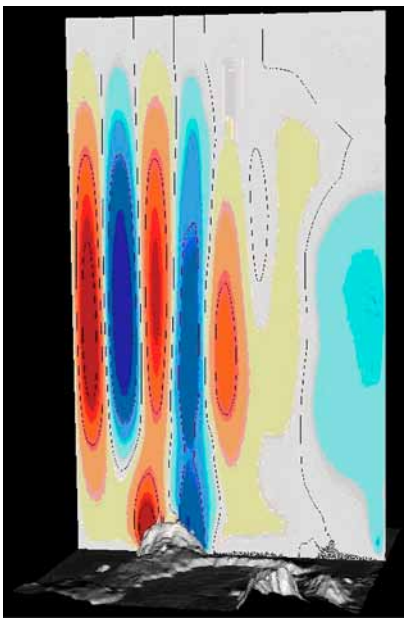

(a) $Fr = 1.0$

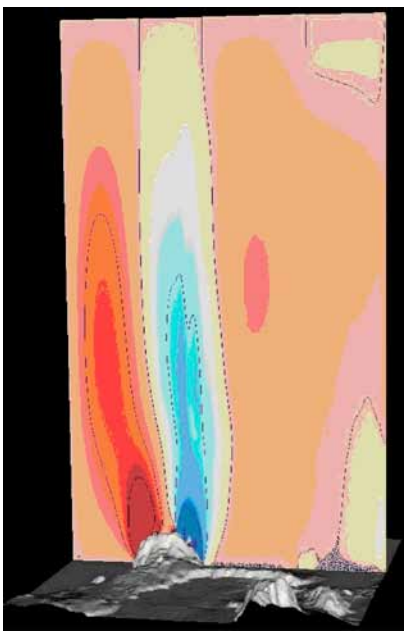

(b) $Fr = 1.5$

Fig. 14. Contours of the vertical velocity component for two different Froude numbers: alternating regions of subsidence and ascent

Acknowledgements

We are thankful to AVINOR for funding the work done in this study. Also we are thankful to Erling Bergersen from AVINOR and Knut Midtbø Helge for their valuable inputs.

References

Bannon, P. 1995. Potential vorticity conservation, hydrostatic adjustment and the anelastic approximation, *Journal of Atmospheric Science* 52: 2302–2312. http://dx.doi.org/10.1175/1520-0469(1995)052<2302:PVCHAA>2.0.CO;2

Clark, T.; Keller, T.; Coen, J., *et al.* 1997. Terrain-induced turbulence over Lantau island: 7 June 1994 tropical storm russ case study, *Journal of Atmospheric Science* 54: 1795–1814. http://dx.doi.org/10.1175/1520-0469(1997)054<1795:TITOLI>2.0.CO;2

Doyle, J.; Durran, D. 2001. The dynamics of mountain-wave-induced rotors, *Journal of Atmospheric Sciences* 59: 186–201. http://dx.doi.org/10.1175/1520-0469(2002)059<0186:TDOMWI>2.0.CO;2

Durran, D. 1998. *Numerical methods for wave equations in geophysical fluid dynamics*. Springer.

Eidsvik, K. 2005. A system of wind power estimation in mountainous terrain prediction of askervein hill data, *Wind Energy* 8(2): 237–249. http://dx.doi.org/10.1002/we.145

Eidsvik, K.; Holstad, A.; Utnes, T. 2004. A prediction system for local wind variation in mountainous terrain, *Boundary Layer Meteorology* 112: 557–586. http://dx.doi.org/10.1023/B:BOUN.0000030561.25252.9e

Plane Crashinfo 2013. *Recent Accidents* [online], [cited 10 August 2013]. Avialable from Internet: http://planecrashinfo.com/.

Rodi, W. 1987. Examples of calculation methods for flow and mixing in stratified fluids, *Journal of Geophysics* 92(C5): 5305–5328. http://dx.doi.org/10.1029/JC092iC05p05305

Utnes, T. 2007a. *A segregated implicit pressure projection method for turbulent flows*: SINTEF Applied Mathematics Report. A1686.

Utnes, T. 2007b. Modelling of stratified geophysical flows over variable topography, *Geometric Modelling, Numerical Simulation and Optimization:* 361–390. ISBN 978-3-540-68782-5.

Utnes, T. 2008. *Effekter av terrengforhyning nr nordlige del av rullebanen p Troms Lufthavn*: SINTEF Applied Mathematics Report. F8246 (in Norwegian).